# Pressure-Induced Conductivity and Yellow-to-Black Piezochromism in a Layered Cu−Cl Hybrid Perovskite

Adam Jaffe,[†,§] Yu Lin,[‡,§] Wendy L. Mao,*[‡] and Hemamala I. Karunadasa*[†]

†Department of Chemistry and ‡Department of Geological and Environmental Sciences, Stanford University, Stanford, California 94305, United States

S *Supporting Information*

ABSTRACT: Pressure-induced changes in the electronic structure of two-dimensional Cu-based materials have been a subject of intense study. In particular, the possibility of suppressing the Jahn−Teller distortion of d^9 Cu centers with applied pressure has been debated over a number of decades. We studied the structural and electronic changes resulting from the application of pressures up to ca. 60 GPa on a two-dimensional copper(II)−chloride perovskite using diamond anvil cells (DACs), through a combination of in situ powder X-ray diffraction, electronic absorption and vibrational spectroscopy, dc resistivity measurements, and optical observations. Our measurements show that compression of this charge-transfer insulator initially yields a first-order structural

(EDBE)[CuCl₄]

phase transition at ca. 4 GPa similar to previous reports on other Cu^II−Cl perovskites, during which the originally translucent yellow solid turns red. Further compression induces a previously unreported phase transition at ca. 8 GPa and dramatic piezochromism from translucent red-orange to opaque black. Two-probe dc resistivity measurements conducted within the DAC show the first instance of appreciable conductivity in Cu^II−Cl perovskites. The conductivity increases by 5 orders of magnitude between 7 and 50 GPa, with a maximum measured conductivity of 2.9×10^{-4} S·cm^{-1} at 51.4 GPa. Electronic absorption spectroscopy and variable-temperature conductivity measurements indicate that the perovskite behaves as a 1.0 eV band-gap semiconductor at 39.7 GPa and has an activation energy for electronic conduction of 0.232(1) eV at 40.2 GPa. Remarkably, all these changes are reversible: the material reverts to a translucent yellow solid upon decompression, and ambient pressure powder X-ray diffraction data taken before and after compression up to 60 GPa show that the original structure is maintained with minimal hysteresis.
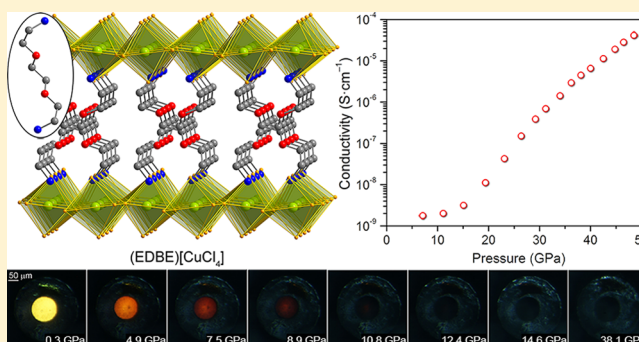
INTRODUCTION

Compression with gigapascal-scale pressures can yield dramatic structural and electronic changes in solids.[1] These include semiconductor-to-metal transitions of low-band-gap organic[2] and inorganic[3] solids, polymerization of conjugated organic groups,[4] spin-polarization reversal,[5] and metal-to-metal charge transfer.[6] In particular, pressure-induced electronic changes of two-dimensional Cu-based solids have been a subject of great interest. This is in part motivated by an attempt to understand the substantial increase in ordering temperature (T_c) observed for high-temperature cuprate superconductors with compression along the copper−oxide planes.[7] Owing to their crystallinity and tunability, two-dimensional Cu−Cl hybrid perovskites[8] are well-defined platforms for studying the evolution of structural and electronic properties with applied pressure. These layered materials consist of corner-sharing sheets of Cu^II−Cl octahedra partitioned by organic cations (Figure 1A), allowing for the compressibility of the inorganic components to be modulated through organic substitution. The 3d^9 Cu^II centers in two-dimensional perovskites show a pronounced Jahn−Teller (JT) distortion owing to the unequal

occupancy of degenerate orbitals in an octahedral ligand field, with long and short Cu−Cl distances of ca. 2.9−3.1 and 2.3 Å, respectively. The elongated axes align in an antiferrodistortive (AFD) arrangement within the plane of the inorganic sheets (Figure 1B). This results in the unpaired electrons residing in orbitals of $dx^2−y^2$ character that have minimal overlap with each other (Figure S2, Supporting Information). Although a half-filled band should provide a conduction pathway, poor overlap between these orbitals likely leads to the materials' insulating nature. Indeed, these materials behave as two-dimensional ferromagnets ($T_c \approx 10$ K)[9] with localized electrons in orthogonal orbitals.

Because applied pressure can both compress and distort the structure, pressure-induced electronic changes in layered hybrid perovskites of the formula $A_2[CuCl_4]$ (A = Rb, Cs, $C_nH_{2n+1}NH_3$; $n = 1–3$) have been intensely investigated. Prior studies have examined structural transitions,[10] evolution of crystal-field states,[11] hole-orbital ordering,[12] changes in
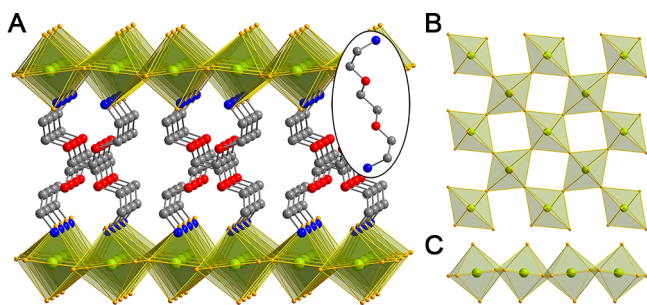
Figure 1. (A) X-ray structure of (EDBE)[CuCl$_4$] (**1**, EDBE = 2,2′-(ethylenedioxy)bis(ethylammonium)). (Inset) EDBE dication. Cu, green; Cl, orange; O, red; N, blue; C, gray. H atoms omitted for clarity. (B) A single inorganic sheet viewed along the *b* axis showing an antiferrodistortive arrangement of the elongated Cl−Cu−Cl axis. (C) View of the inorganic sheets along the *a* or *c* axis.
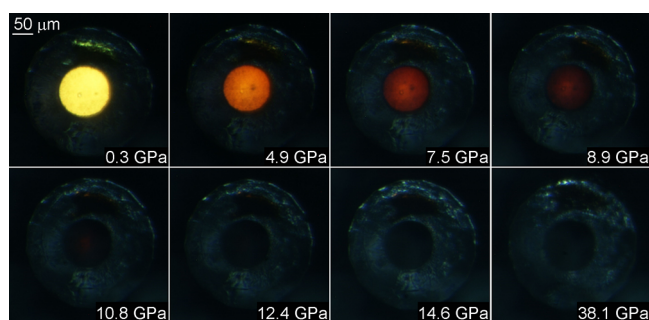

Figure 2. Optical micrographs of **1** in a diamond anvil cell, displaying piezochromic transitions from translucent yellow to red to opaque black.

charge-transfer band energies,[13] and material compressibility.[14] Upon application of hydrostatic pressure, these early studies reported a phase transition at ca. 4 GPa, determined through changes in the Cu−Cl Raman stretching frequencies. This phase transition, which was accompanied by a piezochromic conversion from yellow to red, was initially attributed to complete suppression of the in-plane JT distortion.[10,12] However, later studies that examined electron−phonon coupling constants of the compressed materials and compared local bulk moduli for individual Cu−Cl octahedra with the bulk moduli for the extended structures concluded that the JT distortion should not be suppressed at these pressures.[11,13,14] These studies predicted that the JT distortion should be stable up to ca. 30−40 GPa and that octahedral tilting was the primary avenue for structural evolution under the pressures used (up to 16 GPa).

To the best of our knowledge, effects of higher applied pressures on Cu−Cl perovskites have not been reported. Despite the significant body of work studying pressure-induced changes in these materials, electronic conductivity has not been obtained upon compressing these insulators. Herein, we report the first instance of appreciable conductivity in a layered Cu−Cl perovskite accompanied by dramatic and reversible changes in its optical and electronic properties.

■ RESULTS AND DISCUSSION

Structural Evolution under Pressure. We recently reported the structure of (EDBE)[CuCl$_4$] (**1**, EDBE = 2,2′-(ethylenedioxy)bis(ethylammonium)) (Figure 1A).[15] This perovskite crystallizes in the orthorhombic space group *Pccn* (ambient pressure *α* phase) with adjacent diammonium polyether cations adopting a crossed conformation to afford slight porosity. Upon compression to ca. 4 GPa, **1** displays a similar piezochromic transition to that observed in prior studies for (C$_n$H$_{2n+1}$NH$_3$)$_2$[CuCl$_4$] (*n* = 1−3), from translucent yellow to translucent red (Figure 2). At higher pressures, however, we see previously unreported striking piezochromism. The material darkens upon compression, and above ca. 12 GPa appears opaque black. Notably, this transition is completely reversible: the black color reverts to a bright yellow upon decompression.

To probe the structural evolution under pressure, we recorded high-pressure powder X-ray diffraction (PXRD) patterns of **1** compressed in diamond anvil cells (DACs). We obtained PXRD data up to 6.1 GPa using 600 μm diameter diamond culets and up to 38.6 GPa with 300 μm diameter

diamond culets (Figure 3). The larger culet reaches lower pressures but accommodates a larger sample and finer pressure
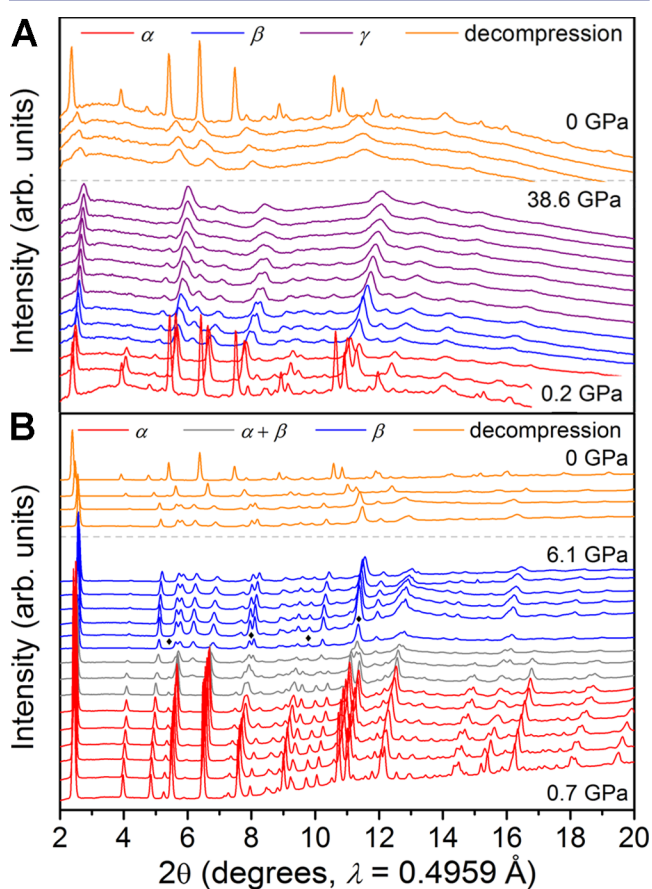
Figure 3. (A) PXRD patterns of **1** upon compression up to 38.6 GPa and decompression to ambient pressure. Data acquired above ca. 8 GPa are shown in purple because EOS fitting indicated a third phase (*γ*). (B) High-resolution PXRD patterns for **1** during compression to 6.1 GPa and decompression to ambient pressure. Black diamonds indicate new or absent reflections in the *β* phase at 3.7 GPa relative to the *α* phase.

steps. Importantly, all observed structural changes are reversible: we obtain the same PXRD patterns at ambient pressure before and after compression up to 60 GPa (Figure S4, Supporting Information). The growth of new peaks and disappearance of some original peaks indicate a phase transition beginning at 3.0 GPa, which is complete by 3.7 GPa (Figure 3B). For example, the (111) reflection centered at 5.47° at
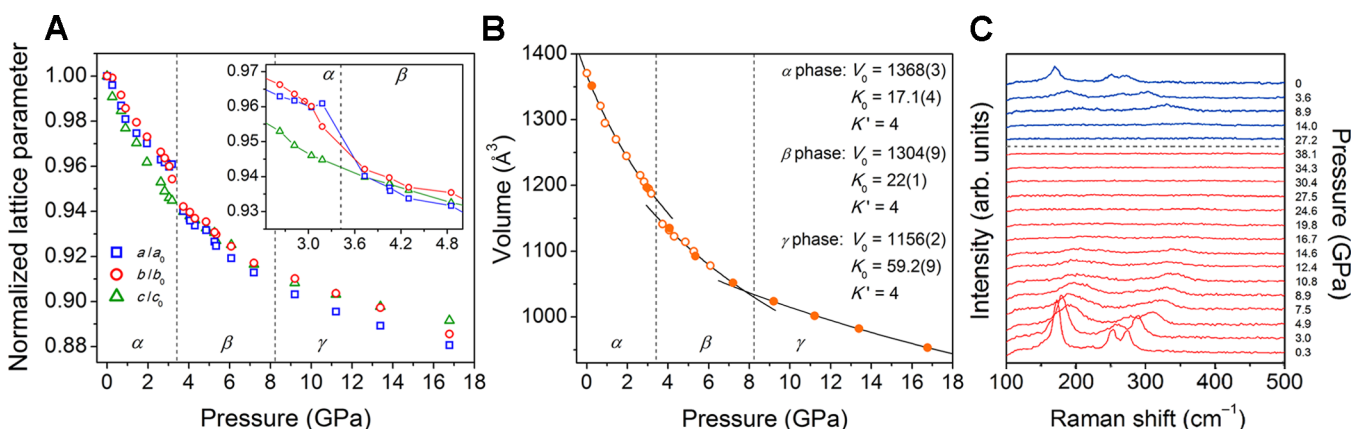
Figure 4. (A) Evolution of lattice parameters of **1** as a function of pressure. (Inset) Magnified region showing lattice parameter behavior at the $\alpha-\beta$ transition. (B) Unit-cell volume changes with pressure. Second-order Birch–Murnaghan (2OBM) EOS fits are shown as black lines. Fit parameters are given for the α, β, and γ phases. Open and closed symbols represent data acquired using a 600 μm culet and a 300 μm culet DAC, respectively. (C) Raman spectra of **1** showing the evolution of Cu–Cl modes upon compression (red lines) and decompression (blue lines).

ambient pressure splits into two reflections at 5.63° and 5.76° at 3.7 GPa. Also, the peak at 7.48° in the ambient-pressure structure resolves into the (200) and (002) reflections at higher pressures within the α phase. The appearance of a reflection at 7.92° at 3.2 GPa indicates the emergence of a second phase (β). When the phase transition is complete at 3.7 GPa, this multiplet splits into Bragg peaks corresponding to the (002) and (210) planes. We used the diffraction pattern obtained at 3.7 GPa to assign the symmetry and determine lattice parameters of the β phase. The two most probable space groups $Pnma$ and $Pnna$ (both orthorhombic with identical unit-cell dimensions) are consistent with the observed reflections and systematic absences. The pressure dependence of the unit-cell dimensions are shown in Figure 4. The sudden volume reduction around 3−4 GPa corroborates a first-order phase transition.

Accounting for compression-induced stiffening in **1**, a fit to the second-order Birch–Murnaghan equation of state (2OBM EOS) for the low-pressure $Pccn$ phase (α phase) yields a K_0 value (bulk modulus at ambient pressure) of 17.1(4) GPa. Variations of K_0 values between the α phases of several Cu–Cl perovskites from ca. 7 to 20 GPa[14] suggest that the organic component plays a templating role in directing the compressibility of the inorganic sheets. The β phase (3.7 GPa to about 7 GPa) is less compressible with a K_0 value of 22(1) GPa. No further discontinuities are apparent in the pressure–volume ($P-V$) profile as pressure is increased above 3.7 GPa. However, we observe a significant change in compressibility between 7 and 9 GPa (Figure 4B), suggesting the occurrence of a second-order, isostructural phase transition. A fit to the 2OBM EOS at and above 9 GPa gives a K_0 value of 59.2(9) GPa for the γ phase. Due to decreased peak intensities and significant peak convolution, we did not determine lattice parameters above 17 GPa.

The c lattice parameter (in plane with respect to the Cu–Cl sheets) decreases nearly monotonically with increasing pressure (Figure 4A). In contrast, a exhibits a sudden decrease at the $\alpha-\beta$ phase transition. Although the c and a directions are equivalent within the Cu–Cl sheets, they differ with respect to the packing of organic molecules. The polyether chains appear more closely packed along the c direction (the viewing direction for Figure 1A), whereas the voids formed by the crossed arrangement of the chains may accommodate greater

compression along the a direction. This indicates that the organic layers can induce anisotropy in the compressibility of the inorganic sheets. The response to compression for each lattice parameter in each phase is summarized in Table 1.

Table 1. Relative Rates of Change in Lattice Parameters during Compression in Each Phase

|	rate of lattice parameter change with pressure, Δ = % change in length/ pressure (GPa^{-1})			
	α phase (0− 3.2 GPa)	$\alpha-\beta$ transition (3.2−3.7 GPa)	β phase (3.7− 7.2 GPa)	γ phase (9.2− 16.8 GPa)
Δa	1.1	4.4	0.8	0.3
Δb	1.4	2.6	0.8	0.4
Δc	1.4	1	0.7	0.2

The high K_0 value of 59.2(9) GPa for the γ phase (compared with 17.1(4) and 22(1) GPa for the α and β phases, respectively) is comparable to the local Cu–Cl octahedron bulk modulus of 63 GPa measured for $(C_3H_7NH_3)_2[CuCl_4]$.[14] This suggests that the overall structure of **1** is sufficiently compressed that further volume reduction for the γ phase occurs mainly in the Cu–Cl octahedra. Using an adaptation of a reported method,[14] we calculated the minimum pressure at which the JT distortion can be completely suppressed: $P_{crit} = E_{JT}/\Delta V$. Here, E_{JT} is the JT stabilization energy and ΔV is the volume change between the initial distorted octahedron and the final undistorted octahedron. Using absorption spectroscopy to determine E_{JT} for **1** as $1/4(a_{1g} \rightarrow b_{1g}$ transition energy),[11] we calculate P_{crit} = 16.7 GPa (see Supporting Information). This provides a lower bound for the pressure required for complete suppression of the JT distortion and further corroborates Cu–Cl octahedron distortions in the γ phase.

We also obtained Raman spectra of **1** under applied pressure to use the Cu–Cl bond stretching frequencies as indicators of altered local geometry for Cu centers. Under ambient pressure we see three peaks at 170, 251, and 270 cm^{-1}, similar to those reported for $(C_2H_5NH_3)_2[CuCl_4]$ at 180, 250, and 280 cm^{-1}. In the prior report, the first two peaks were attributed to Cu–Cl modes and the last peak was assigned to a torsional mode of R–NH$_3$.[10] However, we did not see a shift in these peak positions when we exchanged the hydrogens in the NH$_3$ group with deuterium (Figures S6 and S7, Supporting Information),

which leads us to believe that all three peaks correspond to Cu−Cl modes. This agrees with prior assignments of Raman spectra of similar materials.[17] The three peaks in the Raman spectra of **1** (Figure 4C) remain up to pressures of ca. 8 GPa, though one diminishes more significantly in intensity. These peaks shift toward higher energy, as expected if the Cu−Cl bonds are compressed, and show stress-induced peak broadening. The persistence of the three peaks above 3.7 GPa implies that the JT distortion is not fully suppressed during the first phase transition ($\alpha-\beta$). The two remaining peaks are still weakly visible up to ca. 20 GPa, after which they are no longer discernible over the baseline. At these pressures, we observe that **1** turns opaque black. The black color and flat Raman spectra are consistent with reduced penetration depth of visible light and increased reflectivity in **1**. Similar to the transitions in the PXRD patterns, these changes are also reversible and all three Cu−Cl stretches reappear upon decompression.

Thermochromism and Structural Evolution with Temperature. Yellow crystals of **1** turn bright green at ca. 100 K and red-brown at ca. 350 K, similar to other Cu−Cl perovskites.[16] In order to probe the structural changes that led to these colors, we obtained single-crystal X-ray structures for **1** at 100, 200, 300, and 350 K. All structures were solved in the orthorhombic space group *Pccn*. These data show that the copper coordination environment changes most significantly along three specific outlets (Figure 5 and Table S2, Supporting
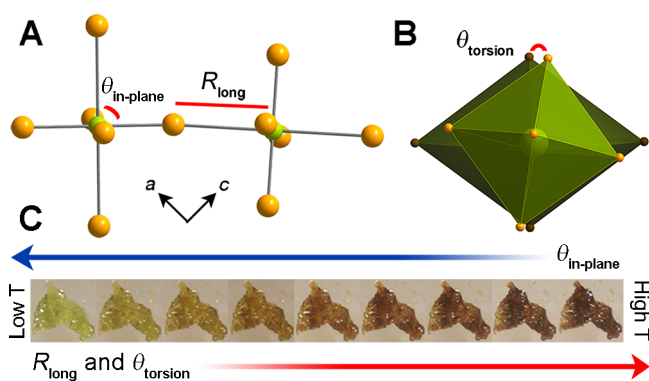

Figure 5. (A) Adjacent octahedra in **1** viewed along the *b* axis (perpendicular to layers). In-plane Cl−Cu−Cl angle and long Cu−Cl bond distance are indicated as $\theta_{\text{in-plane}}$ and R_{long}, respectively. (B) Adjacent octahedra viewed along the [110] direction showing the torsion angle, θ_{torsion}. (C) Variation of R_{long}, $\theta_{\text{in-plane}}$, and θ_{torsion} with thermochromic changes in **1**.

Information). (i) The elongated Cu−Cl bond distance (R_{long}) increases from 3.0568(7) Å at 100 K to 3.114(1) Å at 350 K, whereas there is no change within error in the other Cu−Cl distances. (ii) The in-plane Cl−Cu−Cl angle (i.e., in-plane buckling of the octahedra, $\theta_{\text{in-plane}}$) decreases from 90.00(2)° at 100 K to 89.47(3)° at 350 K, while the other Cl−Cu−Cl angles deviate by 0.2° over the same temperature range. (iii) The torsion angle between octahedra (i.e., the dihedral angle defined by out-of-plane chlorides on adjacent Cu sites, θ_{torsion}) increases from 9.88(2)° to 10.00(4)° between 100 and 350 K. While structural changes induced by temperature and pressure need not be the same, this single-crystal study shows areas of structural lability in **1**. This corroborates the combination of octahedral tilting and Cu−Cl bond compression along the elongated axis as the major avenues of pressure-induced structural changes.

Optical Behavior. The color change from translucent red to opaque black and the loss of peaks in the Raman spectra upon compression indicate large changes in the electronic structure of **1**. We therefore obtained absorption spectra of **1** under pressure using visible and near-IR wavelengths. Solid **1** is a yellow insulator with a ligand-to-metal charge transfer onset at ca. 2.6 eV, similar to other reported Cu−Cl perovskites. This charge-transfer band is assigned to the D_{4h} symmetry-forbidden $a_{2u} \rightarrow b_{1g}$ transition and the symmetry-allowed $e_u \rightarrow b_{1g}$ transition (Figure 6A).[11,18] We determined the band gap of **1** by extrapolating the linear portion of the $(\alpha' \cdot h\nu)^2$ versus $h\nu$ curve in direct band-gap Tauc plots[19] (Figure S9, Supporting Information), where α' is the absorption coefficient, h is Planck's constant, and ν is frequency. It shows a marked red shift from 2.5 eV at 1.0 GPa to 1.0 eV at 39.7 GPa (Figure 6B). At pressures close to 4 GPa, we see an increase in the rate at which the band gap red shifts with pressure, implying that the $\alpha-\beta$ phase transition yields a structure with electronic properties that are more susceptible to compression. Consistent with the occurrence of the second phase transition from β to γ above 9 GPa, another change in the rate of band-gap change occurs between 8 and 10 GPa. At pressures above ca. 10 GPa, when the material starts to convert to the black γ phase, the charge-transfer band edge begins to merge with the d−d transition, which is soon obscured as the charge-transfer band edge moves to IR wavelengths. In the spectra acquired at 9.7, 11.6, and 13.4 GPa, it is therefore more difficult to accurately determine the band-gap energy, leading to the larger uncertainty in band-gap values for these pressures. Overall, applied pressure converts **1** from a charge-transfer insulator at ambient pressure to a semiconductor with a band gap of 1.0 eV at 39.7 GPa.

We also observe a slight blue shift for the peak of the broad d−d band associated with transitions from the a_{1g}, b_{2g}, and e_g orbitals to the b_{1g} orbital (Figures 6B and S14, Supporting Information). Here, the a_{1g} and b_{1g} orbitals are derived from parent e_g orbitals in the idealized Cu−Cl octahedron, while the b_{2g} and e_g orbitals evolve from the degenerate t_{2g} orbitals.[11] Therefore, the holes in the d^9 Cu centers reside in predominantly dx^2-y^2 orbitals (Figure S2, Supporting Information). Because of the antiferrodistortive arrangement of the elongated axes, these half-filled orbitals have no overlap with each other at ambient pressure. Compression of the elongated axes and interoctahedral tilting can relieve the orthogonality of these half-filled orbitals and provide a conduction pathway. Both these structural changes likely contribute to the material's optical and electronic changes in the γ phase.

Electronic Conductivity. We measured the resistivity of **1** as a function of pressure using two-probe dc measurements in a DAC with platinum contacts (Figure 6C, inset). Measurable conductivity occurs at an onset pressure of ca. 7 GPa and steadily increases during compression up to 50 GPa. The electrical conductivity of **1** increases from 1.8×10^{-9} S·cm^{-1} at 7 GPa to 4.1×10^{-5} S·cm^{-1} at 48.5 GPa (Figure 6C). If the cell is allowed to stand over longer time periods, we see further increases in conductivity, reaching a maximum measured conductivity of 2.9×10^{-4} S·cm^{-1} at a slightly increased pressure of 51.4 GPa, most likely from increased interparticle contact. This indicates that conductivity may be limited by poor interparticle contact and/or grain boundary resistance. Variable-temperature measurements (Figure S10, Supporting Information) show that the conductivity follows Arrhenius
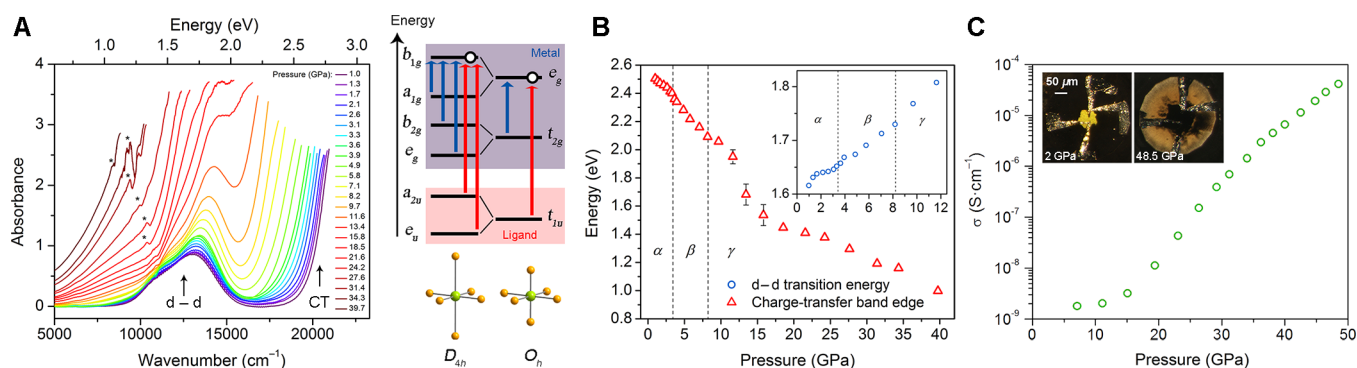
Figure 6. (A) Variable-pressure absorption spectra for **1** using visible and infrared (IR) wavelengths showing the crystal field (d−d) and ligand-to-metal charge transfer (CT) transitions. Asterisks indicate a detector change between visible and IR wavelengths. d−d transitions and CT transitions are shown as blue and red arrows, respectively, in the orbital energy diagrams for D_{4h} and O_h symmetry (from ref 11). Both symmetry allowed and forbidden transitions are shown. (B) CT band-edge energy as a function of pressure calculated from Tauc plots. (Inset) Peak energy of the d−d transition as a function of pressure. (C) Electrical conductivity of **1** as a function of pressure. (Inset) Optical micrographs of a DAC containing **1** contacted by four platinum leads coupled in pairs.

behavior (Figure S11, Supporting Information) with an activation energy for charge transport (E_a) of 0.218(5) eV at 51.4 GPa. Therefore, both absorption and conductivity data indicate that **1** has not achieved a metallic state but behaves as a semiconductor at elevated pressures. Applied pressure likely causes this large increase in conductivity by increasing orbital overlap through reduction in both cell volume as well as local structural distortions.

CONCLUSION

This is the first instance of room-temperature electrical conductivity arising in two-dimensional Cu^{II}−Cl perovskites. Using DACs, we investigated the effects of applying pressures above the theoretical minimum required for suppressing the JT distortion of the d^9 Cu centers. We see dramatic and reversible color changes from translucent yellow to red to opaque black as we apply up to 60 GPa of pressure. Compression of the yellow solid first yields the previously reported first-order phase transition at approximately 4 GPa, when the solid turns translucent red. EOS calculations on pressure-dependent PXRD data show that **1** is a compressible material with a K_0 value of 17.1(4) GPa in the low-pressure α phase. A second, more subtle phase transition occurs between 7 and 9 GPa as characterized by optical absorption and PXRD measurements. Applied pressure above 9 GPa leads to a much less compressible phase with sufficient orbital overlap for charge carrier mobility, requiring that we treat these materials as solids with extended electronic bands. Concomitant with the color change to opaque black, we see a loss of signal in the Raman spectrum and an increase in electrical conductivity of at least 5 orders of magnitude (up to 2.9×10^{-4} S·cm^{−1} at 51.4 GPa) compared to the material at ambient pressure. The band gap of 1.0 eV at 39.7 GPa and temperature dependence of the conductivity ($E_a = 0.232(1)$ eV at 40.2 GPa, Figures S12 and S13, Supporting Information) confirm an activated electronic conduction pathway. The smaller activation energy compared to the band-gap energy suggests that d-orbital bands formed at high pressure contribute to the electronic conduction. Our observations suggest that elevated pressure improves d-orbital overlap by compressing the structure and partially relieves the orthogonality of the half-filled d orbitals through octahedral tilting and Cu−Cl bond compression. Crystal structures obtained at different temperatures where **1** shows thermochro-

mic transitions from green to yellow to red demonstrate that the structure is most labile along these two avenues.

The electronic flexibility of the hybrid perovskite platform has enabled diverse applications as light-emitting diodes,[20] white-light phosphors,[21] and solar-cell absorbers[22] with two-dimensional perovskites, while their three-dimensional analogs have recently shown great promise for photovoltaic[23] and other optoelectronic[24] applications. Our studies on layered perovskite phosphors show that these materials have strong electron−phonon coupling.[21b] Therefore, application of pressure provides an additional tuning knob for accessing further electronic and optical diversity from this exceptionally versatile family of materials.

EXPERIMENTAL METHODS

Crystalline **1** was synthesized according to our previous report.[15] The perovskite samples were compressed using symmetric diamond-anvil cells (DACs) with 300 or 600 μm diameter diamond culets, depending on the measurement (high-pressure Raman, XRD, and optical absorption experiments). A cross-type DAC was used for conductivity measurements. The perovskite samples were loaded into the DACs, and multiple ruby spheres were placed in different locations across the cells for pressure calibration using the ruby fluorescence.[25] High-pressure measurements were acquired without the use of a pressure-transmitting medium, because the soft sample provided acceptable quasi-hydrostatic conditions.

We collected high-pressure Raman spectra on a Renishaw RM1000 Raman microscope using a 514 nm laser excitation line at 1 mW. We performed in situ high-pressure PXRD measurements and variable-temperature single-crystal XRD measurements at beamlines 12.2.2 and 11.3.1, respectively, of the Advanced Light Source (ALS) at the Lawrence Berkeley National Laboratory (LBNL). The PXRD measurements were conducted using 0.4959 Å (25 keV) radiation, and single-crystal measurements were obtained using 0.7749 Å (16 keV) radiation. The PXRD experiments were performed at ambient temperature, while the single-crystal XRD data were obtained at the stated temperatures. The 2D Debye−Scherrer diffraction rings from powder measurements were collected on a Mar345 image plate and integrated using the *FIT2D* software package.[26] The *Jade 5* software package[27] was then employed to index diffraction patterns, determine space groups, and refine structure parameters. Full details of the single-crystal measurements and structure solutions are available in the Supporting Information. We collected high-pressure visible and near-IR absorption spectra at beamline U2A of the National Synchrotron Light Source (NSLS) at Brookhaven National Laboratory (BNL). The visible absorption measurements between 10 000 and 25 000 cm^{−1}

utilized a customized visible microscope system, while the near-IR measurements between 2000 and 11 000 cm^{-1} used a Bruker Vertex 80v FT-IR spectrometer coupled to a Hyperion-2000 microscope with a MCT detector and CaF$_2$ beam splitter.

We performed two-point probe dc conductivity measurements on the samples loaded in DACs by inserting platinum leads (resting on an insulating boron nitride gasket) into the sample cavity. Four platinum leads were inserted in a cross-hair conformation; however, we intentionally touched the leads together in pairs during loading. This way we could verify throughout the experiment that the leads had not been severed by ensuring that there was no resistance between coupled leads. The sample was then loaded into the gasket chamber and compressed. The external leads were connected to a dc resistivity meter (Agilent) or a potentiostat (Bio-Logic VSP 300).

ASSOCIATED CONTENT

Supporting Information

Experimental details, crystallographic information, and spectra. This material is available free of charge via the Internet at http://pubs.acs.org. The CIFs for (EDBE)[CuCl$_4$] at temperatures from 100 to 350 K have been deposited in the Cambridge Crystallographic Data Centre under deposition numbers 1030601, 1030602, 1030603, and 1030604 for structures collected at 100, 200, 300, and 350 K, respectively.

AUTHOR INFORMATION

Corresponding Authors
*wmao@stanford.edu
*hemamala@stanford.edu

Author Contributions
§A.J. and Y.L. contributed equally to this work.

Notes
The authors declare no competing financial interest.

ACKNOWLEDGMENTS

REFERENCES

(1) Tan, J. C.; Cheetham, A. K. *Chem. Soc. Rev.* **2011**, *40*, 1059.

(2) Wong, J. W. L.; Mailman, A.; Lekin, K.; Winter, S. M.; Yong, W.; Zhao, J.; Garimella, S. V.; Tse, J. S.; Secco, R. A.; Desgreniers, S.; Ohishi, Y.; Borondics, F.; Oakley, R. T. *J. Am. Chem. Soc.* **2014**, *136*, 1070.

(3) Nayak, A. P.; Bhattacharyya, S.; Zhu, J.; Liu, J.; Wu, X.; Pandey, T.; Jin, C.; Singh, A. K.; Akinwande, D.; Lin, J.-F. *Nat. Commun.* **2014**, *5*, 3731 DOI: 10.1038/ncomms4731.

(4) Murli, C.; Song, Y. *J. Phys. Chem. B* **2010**, *114*, 9744.

(5) Pfleiderer, C.; McMullan, G. J.; Julian, S. R.; Lonzarich, G. G. *Phys. Rev. B* **1997**, *55*, 8330.

(6) Huang, Z.; Auckett, J. E.; Blanchard, P. E. R.; Kennedy, B. J.; Miiller, W.; Zhou, Q.; Avdeev, M.; Johnson, M. R.; Zbiri, M.; Garbarino, G.; Marshall, W. G.; Gu, Q.; Ling, C. D. *Angew. Chem., Int. Ed.* **2014**, *53*, 3414.

(7) (a) Gao, L.; Xue, Y. Y.; Chen, F.; Xiong, Q.; Meng, R. L.; Ramirez, D.; Chu, C. W.; Eggert, J. H.; Mao, H. K. *Phys. Rev. B* **1994**, *50*, 4260. (b) Murayama, C.; Iye, Y.; Enomoto, T.; Môri, N.; Yamada, Y.; Matsumoto, T.; Kubo, Y.; Shimakawa, Y.; Manako, T. *Physica C* **1991**, *183*, 277. (c) Schilling, J. S. In *Frontiers of High Pressure Research II: Application of High Pressure to Low-Dimensional Novel Electronic Materials*; Hochheimer, H. D., Kuchta, B., Dorhout, P. K., Yarger, J. L., Eds.; Springer: New York, 2001; Vol. 48, p 345.

(8) Mitzi, D. B. *Prog. Inorg. Chem.* **1999**, *48*, 1.

(9) de Jongh, L. J.; Botterman, A. C.; de Boer, F. R.; Miedema, A. R. *J. Appl. Phys.* **1969**, *40*, 1363.

(10) Moritomo, Y.; Tokura, Y. *J. Chem. Phys.* **1994**, *101*, 1763.

(11) Valiente, R.; Rodríguez, F. *Phys. Rev. B* **1999**, *60*, 9423.

(12) Ohwada, K.; Ishii, K.; Inami, T.; Murakami, Y.; Shobu, T.; Ohsumi, H.; Ikeda, N.; Ohishi, Y. *Phys. Rev. B* **2005**, *72*, 014123.

(13) Rodríguez, F.; Aguado, F.; Valiente, R.; Hanfland, M.; Itiè, J. P. *Phys. Status Solidi B* **2007**, *244*, 156.

(14) Aguado, F.; Rodríguez, F.; Valiente, R.; Itiè, J.-P.; Hanfland, M. *Phys. Rev. B* **2012**, *85*, 100101.

(15) Jaffe, A.; Karunadasa, H. I. *Inorg. Chem.* **2014**, *53*, 6494.

(16) Birrell, G. B.; Zaslow, B. *J. Inorg. Nucl. Chem.* **1972**, *34*, 1751.

(17) (a) Beattie, I. R.; Gilson, T. R.; Ozin, G. A. *J. Chem. Soc. A* **1969**, 534. (b) Smith, D. W. *Coord. Chem. Rev.* **1976**, *21*, 93.

(18) Desjardins, S. R.; Wilcox, D. E.; Musselman, R. L.; Solomon, E. I. *Inorg. Chem.* **1987**, *26*, 288.

(19) Tauc, J. *Mater. Res. Bull.* **1968**, *3*, 37.

(20) (a) Chondroudis, K.; Mitzi, D. B. *Chem. Mater.* **1999**, *11*, 3028. (b) Era, M.; Morimoto, S.; Tsutsui, T.; Saito, S. *Appl. Phys. Lett.* **1994**, *65*, 676.

(21) (a) Dohner, E. R.; Hoke, E. T.; Karunadasa, H. I. *J. Am. Chem. Soc.* **2014**, *136*, 1718. (b) Dohner, E. R.; Jaffe, A.; Bradshaw, L. R.; Karunadasa, H. I. *J. Am. Chem. Soc.* **2014**, *136*, 13154.

(22) Smith, I. C.; Hoke, E. T.; Solis-Ibarra, D.; McGehee, M. D.; Karunadasa, H. I. *Angew. Chem., Int. Ed.* **2014**, *53*, 11232.

(23) (a) Green, M. A.; Ho-Baillie, A.; Snaith, H. J. *Nat. Photonics* **2014**, *8*, 506. (b) Kazim, S.; Nazeeruddin, M. K.; Grätzel, M.; Ahmad, S. *Angew. Chem., Int. Ed.* **2014**, *53*, 2812.

(24) (a) Xing, G.; Mathews, N.; Lim, S. S.; Yantara, N.; Liu, X.; Sabba, D.; Grätzel, M.; Mhaisalkar, S.; Sum, T. C. *Nat. Mater.* **2014**, *13*, 476. (b) Deschler, F.; Price, M.; Pathak, S.; Klintberg, L. E.; Jarausch, D.-D.; Higler, R.; Hüttner, S.; Leijtens, T.; Stranks, S. D.; Snaith, H. J.; Atatüre, M.; Phillips, R. T.; Friend, R. H. *J. Phys. Chem. Lett.* **2014**, *5*, 1421. (c) Tan, Z.-K.; Moghaddam, R. S.; Lai, M. L.; Docampo, P.; Higler, R.; Deschler, F.; Price, M.; Sadhanala, A.; Pazos, L. M.; Credgington, D.; Hanusch, F.; Bein, T.; Snaith, H. J.; Friend, R. H. *Nat. Nanotechnol.* **2014**, *9*, 687.

(25) Mao, H. K.; Xu, J.; Bell, P. M. *J. Geophys. Res. B* **1986**, *91*, 4673.

(26) Hammersley, A. P.; Svensson, S. O.; Hanfland, M.; Fitch, A. N.; Hausermann, D. *High Pressure Res.* **1996**, *14*, 235.

(27) *Jade 5.0*; Materials Data Inc.: Livermore, CA, 1998.